frontiers in
COMPUTATIONAL NEUROSCIENCE

ORIGINAL RESEARCH ARTICLE
published: 28 December 2010
doi: 10.3389/fncom.2010.00157

Decorrelation of odor representations via spike timing-dependent plasticity

Christiane Linster*[1,2] *and Thomas A. Cleland*[1,3]

[1] *Computational Physiology Laboratory, Cornell University, Ithaca, NY, USA*
[2] *Department of Neurobiology and Behavior, Cornell University, Ithaca, NY, USA*
[3] *Department of Psychology, Cornell University, Ithaca, NY, USA*

Edited by:
Wulfram Gerstner, Ecole Polytechnique Fédérale de Lausanne, Switzerland

Reviewed by:
Guillaume Hennequin, Ecole Polytechnique Fédérale de Lausanne, Switzerland

***Correspondence:**
Thomas A. Cleland, Department of Psychology, Cornell University, Ithaca, NY 14853, USA.
e-mail: thomas.cleland@cornell.edu

The non-topographical representation of odor quality space differentiates early olfactory representations from those in other sensory systems. Decorrelation among olfactory representations with respect to physical odorant similarities has been proposed to rely upon local feed-forward inhibitory circuits in the glomerular layer that decorrelate odor representations with respect to the intrinsically high-dimensional space of ligand–receptor potency relationships. A second stage of decorrelation is likely to be mediated by the circuitry of the olfactory bulb external plexiform layer. Computations in this layer, or in the analogous interneuronal network of the insect antennal lobe, are dependent on fast network oscillations that regulate the timing of mitral cell and projection neuron (MC/PN) action potentials; this suggests a largely spike timing-dependent metric for representing odor information, here proposed to be a precedence code. We first illustrate how the rate coding metric of the glomerular layer can be transformed into a spike precedence code in MC/PNs. We then show how this mechanism of representation, combined with spike timing-dependent plasticity at MC/PN output synapses, can progressively decorrelate high-dimensional, non-topographical odor representations in third-layer olfactory neurons. Reducing MC/PN oscillations abolishes the spike precedence code and blocks this progressive decorrelation, demonstrating the learning network's selectivity for these sparsely synchronized MC/PN spikes even in the presence of temporally disorganized background activity. Finally, we apply this model to odor representations derived from calcium imaging in the honeybee antennal lobe, and show how odor learning progressively decorrelates odor representations, and how the abolition of PN oscillations impairs odor discrimination.

Keywords: olfaction, gamma oscillations, sparse synchronization, STDP, olfactory bulb, antennal lobe, odor learning, conditioning

INTRODUCTION

As neural representations of sensory stimuli progress from peripheral sensors into the central nervous system, they are transformed not only in terms of feature selectivity but also in terms of the underlying spike encoding metric. Specifically, whereas neurons embedded in primary sensory organs appear to represent information largely by "rate coding" – a simple metric in which the instantaneous spike rate of a cell represents its level of activation, and the timecourse of activity follows that of the stimulus – higher-order sensory neurons can transform this information into more sophisticated metrics, with evoked action potentials typically sparser in terms of total activity and more tightly regulated in time (*temporal precision*; Panzeri et al., 2009). In particular, the coordinated regulation of action potential timing within and among regions of the brain is associated with fast oscillations in the local field potential (LFP) that exhibit frequencies of 15–100 Hz (i.e., in the beta and gamma bands). Fast LFP oscillations are observed in visual cortex (Gray and Singer, 1989; Nase et al., 2003), in the olfactory systems of vertebrates (Buonviso et al., 2003; Neville and Haberly, 2003; Lagier et al., 2004; David et al., 2009) and insects (Laurent and Davidowitz, 1994; Stopfer et al., 1997; Cassenaer and Laurent, 2007), as well as broadly across associational areas including hippocampus and isocortex (Sirota et al., 2008; Hajos and Paulsen, 2009). In the honeybee olfactory system, the disruption of coordinated oscillations in the antennal lobe (AL) reduces sensory acuity and broadens generalization among similar odors (Stopfer et al., 1997). In the analogous mammalian olfactory bulb (OB), the enhancement of oscillations has been associated with increased perceptual acuity (Nusser et al., 2001; Beshel et al., 2007; Kay et al., 2009); moreover, olfactory acuity is impaired by reducing inhibitory synaptic strengths in the recurrent circuit from which gamma oscillations are generated, and enhanced by the potentiation of this inhibition (Abraham et al., 2010). That is, in this system, and perhaps generally, spike timing regulation appears not to replace but to supplement and modify the specificity of the underlying identity code, in which chemosensory information is represented by the identities of the ensemble of spiking projection neurons (reviewed by Laurent, 1999) – or, more precisely, by the pattern of relative levels of activation across the ensemble (Cleland et al., 2007).

There are multiple metrics by which information can be represented via the regulation of spike timing (Hopfield, 1995; Masquelier et al., 2009; Panzeri et al., 2009). One of the biophysically simplest of these utilizes *precedence coding*, a term that reflects both the *latency code* and *phase code* described by Panzeri et al. (2009). In precedence coding, information about the level of neuronal activation is converted into relative spike latency, such that neurons that are more

strongly activated generate correspondingly shorter-latency spikes – i.e., a given spike's precedence with respect to the ensemble of its peers signals the relative strength or importance of its signal. Prerequisite to such a code, however, is a common time reference among all neurons participating in the representation. This reference can originate from a single, common external event such as an experimental stimulus presentation or active sampling behavior – in tetrapod olfaction, the latter corresponds to a sniff (Schaefer and Margrie, 2007; Wachowiak et al., 2009), whereas in arthropods antennal flicking appears to serve a similar purpose (Koehl et al., 2001). Alternatively, or additionally, the time reference can be a shared internal clock such as is indicated by the presence of fast LFP oscillations (Fries et al., 2007); indeed, oscillatory coherence within and among cortical structures has been clearly associated with sensory activation and selective attention to stimuli (Kay and Freeman, 1998; Martin et al., 2007; Uhlhaas et al., 2009; Ardid et al., 2010). In this context, precedence codes reflect the phase precedence of each neuron's spiking with respect to the periodically distributed collective activity of its peers, as can be estimated by measuring the LFP oscillation.

Direct evidence for the functional importance of precedence codes in fast oscillations is rare but accumulating. The relative phase lead of evoked spikes in primary visual cortex neurons corresponds to the strengths of their excitatory drives (reviewed in Fries et al., 2007) and can be exploited to create sparse representations when paired with a spike timing-dependent plasticity rule, as proposed by Thorpe and colleagues (Guyonneau et al., 2005; Masquelier et al., 2009). In an odor-activated subset of mitral cells in the rodent OB, spikes are sharply phase-constrained with respect to underlying gamma oscillations, and the phase of spiking in a given cell can persist across multiple gamma cycles (David et al., 2009). While there is no direct evidence regarding whether or not the spike timing-sensitivity of second-order olfactory principal neurons reflects such a precedence code, theoretical work based on OB slice recordings does suggest that spike precedence in activated mitral cells, coordinated in time by an input-induced phase reset in their subthreshold oscillations, will directly reflect their presynaptic activation levels (Desmaisons et al., 1999; Rubin and Cleland, 2006). We here outline a model framework in which odor representations embedded in OB/AL spike precedence codes can be read and appropriately interpreted by spike timing-dependent computations that systematically modify synaptic weights and construct sparse representations in the next neuronal layer.

The model is predicated on the common architectural principles of complex olfactory systems in vertebrates and arthropods, as illustrated in **Figure 1A**. Briefly, a population of odor-selective primary olfactory sensory neurons (OSNs) in the sensory periphery responds to odorant stimuli, the axons of these OSNs project to the OB/AL and segregate therein into discrete glomeruli on the basis of their chemoreceptive fields; i.e., each glomerulus directly inherits the chemoreceptive field of its constituent OSNs. Second-order principal neurons (e.g., mitral cells, projection neurons) are excited by OSN activity, though their spiking output is substantially shaped by intrinsic inhibitory interneurons, resulting in the decorrelation of different odor representations and the phase-constraining of MC/PN spiking with respect to a periodic beta/gamma-band clock. While several factors, both intrinsic and learned, contribute to the regulation of olfactory decorrelation in the OB (reviewed in Cleland et al. 2009; Mandairon and Linster, 2009), we here focus specifically on the regulation of MC/PN spiking activity by intrabulbar oscillatory dynamics and how odor representations based upon spike precedence coding could be utilized by postbulbar computations.

MATERIALS AND METHODS

NETWORK ARCHITECTURE

The model architecture is depicted in **Figure 1A**. To minimize free parameters and facilitate systematic analysis, we used simplified neuron models and a reduced version of the OB/AL network. A total of 100 glomeruli, including associated OSNs and mitral cells (MCs; or, equivalently, insect projection neurons, PNs) were simulated and arranged for display in a two-dimensional 10×10 array (spatial location in this array had no influence on computations). Simulated odorants each activated characteristic, arbitrary subgroups of model OSNs to differing degrees. Specifically, each model OSN exhibited a normally distributed receptive field with a ligand–receptor potency value for each odorant drawn randomly from this distribution. The statistical distribution of OSN receptive fields was random with respect to location across the 10×10 array. Glomerular-layer computations were not explicitly simulated; as this circuitry is thought to perform initial decorrelation operations and limit the range of absolute activity levels among MC/PNs (Linster et al., 2005; Cleland, 2010), its effect can be approximated by appropriately limiting the range of model odorant stimuli presented to the model. Model MC/PNs received direct synaptic excitation from the OSN population associated with a given glomerulus (modeled in aggregate) as well as periodic feedforward inhibition from a non-spiking interneuron representing a population of interconnected inhibitory interneurons (e.g., vertebrate granule cells or insect homoLN interneurons). (The network mechanisms responsible for generating fast oscillations in the OB and AL are contested, and it is not the goal of the present model to explore their relative merits). The single interneuron implemented herein (GC/hLN) received excitatory input from all OSNs and fed inhibition back onto itself as well as delivering inhibition onto all MC/PNs. This connectivity resembles that described in the insect AL, in which oscillatory activity is thought to be generated by a network of inhibitory local interneurons (MacLeod and Laurent, 1996; Stopfer et al., 1997); in the olfactory bulb, fast oscillations also depend on inhibitory synaptic interactions, although granule cells receive their afferent activation indirectly (via mitral cells). This autoinhibitory feedback loop generated stimulus-evoked gamma-band oscillations in the GC/hLN interneuron that also phase-constrained the spike timing of MC/PNs via periodic inhibition (**Figure 1B**). MC/PNs in turn projected excitatory, plastic synapses onto a second 10×10 layer of principal neurons representing higher processing centers such as piriform cortical pyramidal cells (PCs) or insect mushroom body Kenyon cells. The projection matrix between MC/PNs and PCs was sparse (5% connectivity), uniformly distributed, and randomized (Linster et al., 2007, 2009), and generated sparse, distributed, and plastic patterns of odor-responsive activity in PNs after conditioning (**Figure 1C**), as has been observed in rodent piriform cortex (Johnson et al., 2000; Illig and Haberly, 2003; Roesch et al., 2007; Poo and Isaacson, 2009; Stettler and Axel, 2009). Synaptic connections and parameter values are presented in **Table 1**.

MODEL NEURON EQUATIONS

All neurons were represented as single compartments; each compartment was characterized by a membrane time constant that can be regarded as the mean product of the membrane capacitance and the membrane input resistance. Consequently, the evolution of the membrane voltage over time is described by a first order differential equation:

$$\tau \frac{dv(t)}{dt} + v(t) = I_{ext}(t), \quad (1)$$

where τ is the charging time constant of the neuron and $I_{ext}(t)$ is the total input at time t.

MC/PN and PC neurons produced discrete spikes of unit amplitude for output, computed according to the instantaneous spiking probability, a continuous, bounded function of the membrane potential with a threshold θ_{min} and a saturation value θ_{max}. The instantaneous spiking probability $P(x = 1)$ was 0 below the threshold, varied linearly between the threshold and saturation and was 1.0 above saturation. Membrane potential was reset to rest after each spike.

$$\begin{aligned} &P(x=1) = 0 \text{ if } v(t) \le \theta_{min} \\ &P(x=1) = (v(t) - \theta_{min})/(\theta_{max} - \theta_{min}) \text{ if } \theta_{min} < v(t) < \theta_{max} \\ &P(x=1) = 1 \text{ if } v(t) \ge \theta_{max} \end{aligned} \quad (2)$$

The inhibitory interneuron was a non-spiking interneuron with a continuous output variable. The interneuron output was calculated according to the same continuous, bounded function of the membrane potential:

$$\begin{aligned} &x(t) = 0 \text{ if } v(t) \le \theta_{min} \\ &x(t) = (v(t) - \theta_{min})/(\theta_{max} - \theta_{min}) \text{ if } \theta_{min} < v(t) < \theta_{max} \\ &x(t) = 1 \text{ if } v(t) \ge \theta_{max} \end{aligned} \quad (3)$$

The input to a postsynaptic neuron i from a particular presynaptic neuron j at time t was computed as a function of the synaptic strength w_{ij}, the conductance change $g(t)$ due to a presynaptic output event x_j (either a unitary event representing an action potential or an analog value in the case of the inhibitory interneuron), and the difference between the Nernst potential $E_{N,ij}$ of the associated synaptic channel and the current membrane potential v_i of the postsynaptic neuron:

$$I_{i,ext}(t) = \sum_j W_{ij} \sum_{tj<t} g(t - t_j)\left[E_{N,ij} - V_i(t)\right] \quad (4)$$

The time course of g was described by a double exponential function:

$$g(t - t_j) = g_{max} \frac{\tau_1 \tau_2}{\tau_1 - \tau_2}\left(e^{-(t-t_j)/\tau_1} - e^{-(t-t_j)/\tau_2}\right) \quad (5)$$

DECORRELATION CALCULATIONS

To calculate the overlap between representations and thereby measure the effectiveness of decorrelation, 80 simulations, each using a new pair of randomly determined odorants, were run for each of two conditions: a normal oscillatory condition and a condition in which oscillations were suppressed so as to eliminate MC/PN precedence coding. Odor representations at each level of the network were represented by 100-element activity vectors in which each element represented the average output activity of the corresponding MC/PN or PC pyramidal neuron over the course of a 500-ms stimulation. The overlaps between the representations of each odor stimulus pair by the MC/PN and PC ensembles were calculated as the normalized dot product between the corresponding 100-element activity vectors O_1 and O_2:

$$\text{Overlap}_{O_1,O_2} = \frac{\sum_{i=1}^{N} O_{1i} O_{2i}}{||O_1|| ||O_2||} \quad (6)$$

where O_{1i},O_{2i} are the elements of the activity vectors O_1 and O_2, respectively, and $||O_1||$, $||O_2||$ are the norms of vectors O_1 and O_2. Activity vectors were computed from the numbers of spikes evoked in each neuron during the time of stimulus application.

STDP LEARNING RULE

The strengths of synaptic inputs from MC/PNs to PCs were each set to a baseline value w_{PC} when the network was created. During the odor conditioning phase, the strengths of these synapses were altered according to a spike timing-dependent plasticity (STDP) learning rule (**Figure 1D**). The degree of synaptic modification depends on the relative timing between pre- and post-synaptic action potentials, according to a function $F(\Delta t)$ of the time Δt between the presynaptic (MC/PN) and postsynaptic (PC) spikes, such that:

$$F(\Delta t) = \begin{cases} A_+ \exp(\Delta t/\tau_+) & \text{if } \Delta t < 0 \\ A_- \exp(-\Delta t/\tau_-) & \text{if } \Delta t > 0 \end{cases} \quad (7)$$

That is, when a presynaptic spike precedes the postsynaptic spike, the associated synapse becomes strengthened in a manner that depends on the time delay between the two spikes. Similarly, when the presynaptic spike follows the postsynaptic spike, the synapse is weakened (**Figure 1D**). Synaptic strength changes depend on all spike combinations within the time constant of the rule, not only nearest neighbors. The conditioning phases were short enough so that reinforced weights did not grow excessively large. Since synapses undergoing reinforcement were excitatory, synaptic weights were not allowed to decrease below 0.

When constructing each network, all parameters were chosen from a randomized uniform distribution of ±10% around the mean values listed in **Table 1**. Cellular resting potentials were set to 0 mV and ionic Nernst potentials were adjusted accordingly. The associative learning rule time constants τ_+ and τ_- were the same for all model neurons (**Table 1**; **Figure 1D**). Two conditions were simulated: (a) a condition in which the inhibitory interneuron generated a stable, fast network oscillation due to inhibitory feedback in the GC/hLN interneuron and (b) a condition in which this feedback inhibition was reduced such that stable oscillations did not occur. The net inhibition delivered onto the MC/PN population was also reduced in the latter condition so as to maintain similar overall firing rates in these neurons in response to olfactory input (**Figure 1E**).

RESULTS

STDP RULE RESPONDS TO PRECEDENCE CODES

The STDP rule is inherently sensitive to spike timing, and its temporal stringency can be arbitrarily adjusted by altering the values of τ_+ and τ_- (Eq. 7; **Figure 1D**). Moreover, its asymmetry around the time of the postsynaptic spike suggests a proclivity for "edge enhancement" akin to the ubiquitous Mexican-hat decorrelation function but operating with respect to a spike timing-based metric. That is, incoming spike times preceding the postsynaptic spike constitute the central peak of the receptive field and are consequently strengthened, and spike times immediately following the postsynaptic spike – i.e., immediately adjacent to the edge of the representation – constitute the "inhibitory surround" and are specifically weakened.

As proof of concept, we modeled a postsynaptic neuron receiving incoming spikes from 10 presynaptic neurons; these 10 neurons were differentially activated so as to each evoke a spike at a different time. Initially, the synaptic integration properties of the postsynaptic neuron were set such that the first six spikes arriving within a 10 ms window would evoke a postsynaptic action potential (**Figure 1D**, left); hence, the corresponding six synapses were strengthened (*blue*) and the remaining four weakened (*red*) by the STDP rule. After a period of conditioning, the potentiated synapses evoked a postsynaptic spike after only five of the presynaptic neurons had fired, because fewer of these strengthened inputs were required to evoke that spike. The neuron firing sixth consequently had its synaptic weight dramatically weakened – even though it had been the strongest synapse up until that point – and thereafter became excluded from the relevant presynaptic representation (i.e., it effectively lost the capacity to influence the activity of the postsynaptic neuron). This progressive sharpening, and the concomitant functional "pruning" of synapses, proceeded in response to continued conditioning

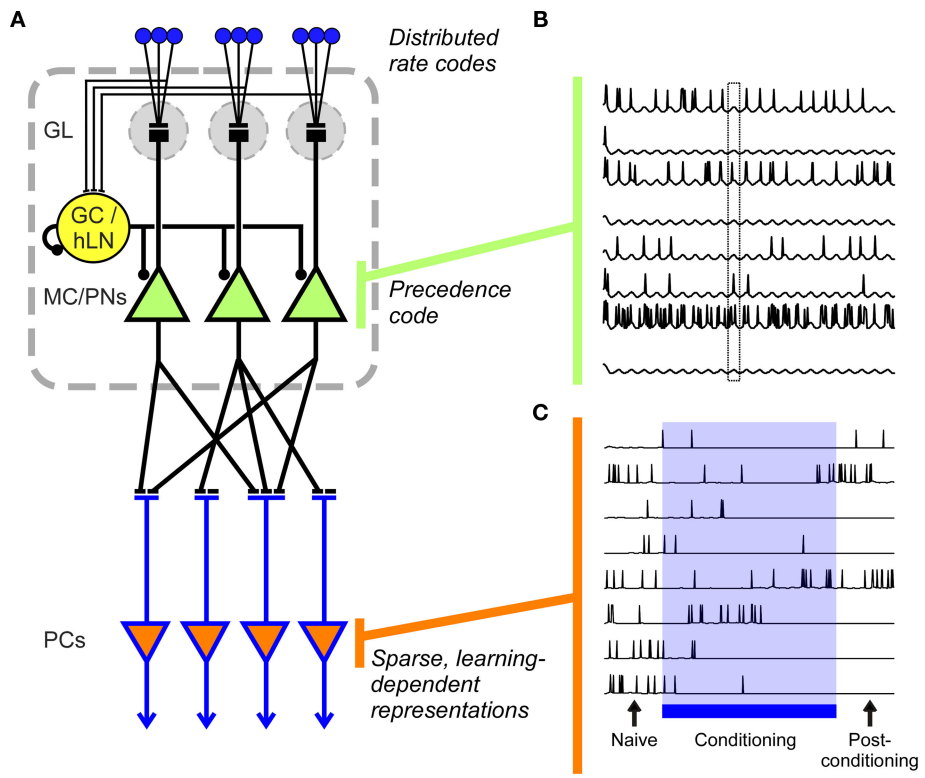

FIGURE 1 | Precedence coding in a model of vertebrate olfactory bulb/insect antennal lobe (OB/AL). (A) Model architecture. In the model, OSNs, each expressing a specific distribution of sensitivities to simulated odorants, project to principal neurons: mitral cells (MCs) in the OB or projection neurons (PNs) in the AL. A single local interneuron (GC/hLN), corresponding to a population of local inhibitory neurons (granule cells in the OB, homoLNs in the AL), also receives excitatory input from the OSNs. (In the OB, the corresponding excitation of deep-layer interneurons is indirect, whereas in the AL these interneurons are directly activated by OSNs). MC/PN neurons project to principal neurons in the next layer, corresponding to insect mushroom bodies or vertebrate piriform cortex (PC) with a sparse but uniform probability. The MC/PN synapses onto PC neurons are plastic according to the STDP learning rule. GL, glomerular layer; MC/PNs, mitral cells/projection neurons; PCs, piriform pyramidal neurons/mushroom body Kenyon cells. **(B)** MC/PN spiking patterns are shaped by global oscillatory dynamics. Periodic inhibitory input from the local interneuron phase-constrains spikes from odor-activated MC/PNs such that a precedence code is established in which the most strongly activated cells tend to spike early in the oscillation period (phase lead). Traces from eight differentially activated MC/PNs are depicted. The *box outline* highlights the difference in spike phase among three different activated neurons. **(C)** PC neurons respond broadly to odors before conditioning and generate a sparse and robust representation after conditioning. Initial uniform (5%) connectivity (*Naïve*) results in relatively weak and broadly distributed odor responses in PC neurons. During the conditioning phase (*Conditioning*), the distribution of synaptic weights between MC/PNs and PC is progressively adjusted via the STDP learning rule, eventually yielding a sparse, robust distribution of odor responses across the PC population (*Post-conditioning*). Note that during the conditioning process, individual PC odor responses may evolve non-monotonically; some PCs may at first be suppressed by learning but then become part of the durably activated ensemble (e.g., second trace), whereas others may initially be potentiated in their responses but in the end be excluded from the odor-specific ensemble (e.g., sixth trace).

(continued)

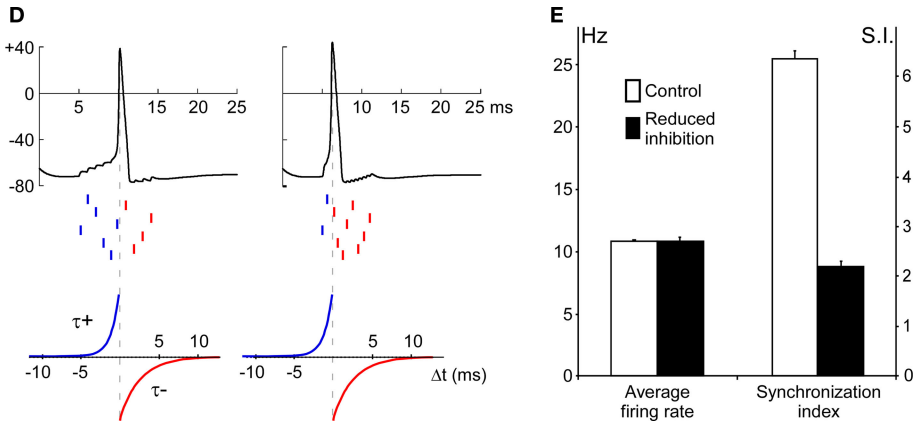

FIGURE 1 | Precedence coding in a model of vertebrate olfactory bulb/insect antennal lobe (OB/AL). (D) Mechanism underlying decorrelation of precedence-coded neural representations via the STDP learning rule. Left: Ten presynaptic MC/PN neurons deliver spikes (*middle raster marks*) to a postsynaptic PC neuron (*top trace*) within a ~10 ms phase window. Here, the PC neuron accumulates inputs and fires an action potential after the sixth presynaptic spike. According to the STDP learning rule (*bottom*; Song et al., 2000), the synapses from the presynaptic neurons associated with the first six spikes should be potentiated (*blue*), with the synapse associated with the sixth spike being the most strongly potentiated and the synapse associated with the first spike being relatively weakly potentiated if at all. The synapses associated with the four latest spikes are all weakened (*red*; corresponding to the negative region of the STDP rule in the bottom panel). This potentiation of the first six synapses will lead to the progressively earlier evocation of the postsynaptic PC spike; i.e., once the first five potentiated synaptic inputs suffice to evoke the postsynaptic spike, the synapse from the sixth-firing neuron will be powerfully weakened – even though it had previously been the most strongly potentiated – and eventually that MC/PN neuron will be excluded from the effective presynaptic ensemble. *Right panel.* Higher odorant concentrations evoke higher-power oscillations and more tightly phase-constrained presynaptic action potentials (discussed in Cleland and Linster, 2002); these tightly synchronized spikes integrate more effectively in postsynaptic neurons such that spikes from fewer neurons are required to evoke a postsynaptic action potential, all else being equal. This has the intrinsic effect of increasing the rate of synaptic learning; i.e., the rate at which the postsynaptic spike time phase-advances to exclude increasing numbers of MC/PNs from the effective presynaptic representation (i.e., the set of MC/PN cells with synaptic weights sufficient to affect the activity of the postsynaptic neuron). Interestingly, this effect of stimulus intensity on learned representations is in accord with classical learning theory (discussed in Cleland et al., 2009). Dotted vertical lines represent the spike time for purposes of the STDP rule. Ordinates in the top panels represent membrane potential in millivolts. **(E)** Average spike rate (Hz) and synchronization among MC/PN neurons during control and reduced-inhibition conditions. The synchronization index was calculated as the number of pairs of spikes occurring within 1 ms of each other divided by the total number of spikes (Linster and Cleland, 2001).

until an asymptotically minimal effective ensemble was reached. Interestingly, spike series that are more tightly constrained in time, such as are associated with higher-concentration odorant stimuli evoking higher-power oscillations (Cleland and Linster, 2002), intrinsically generate sharper representations by this metric. That is, all else being equal, they are able to evoke postsynaptic spikes with fewer presynaptic spikes so as to more rapidly exclude neurons from the presynaptic representation, essentially increasing the rate of conditioning (**Figure 1D**, right). Notably, olfactory psychophysical experiments in mice have shown that presenting higher-concentration odorants both increases the rate of conditioning and generates sharper odor representations, as this model predicts (Cleland et al., 2009).

NAÏVE ODOR RESPONSES IN MODEL PC ARE BROAD AND POORLY SELECTIVE

We then constructed a larger-scale network model of the vertebrate olfactory bulb/insect antennal lobe (OB/AL) to measure the capacity of this STDP implementation to progressively sharpen odor representations in the PC layer, and specifically to measure the selectivity of this conditioning mechanism for spike precedence-based representations in MC/PNs even in the presence of temporally uncoordinated background spiking. First, we measured the capacity of the STDP learning rule to extract precedence codes from the MC/PN cell layer in order to create representations in the PC layer. Broad, complex odorant stimuli were designed to activate a large proportion of OSNs in order to better visualize the progression of olfactory decorrelation in the model (**Figure 2A**, OSNs). The action potentials of MC/PNs that responded to odor stimulation with increased firing rates were strongly phase-modulated by the underlying fast oscillations. While the OB circuitry explicitly implementing glomerular-layer decorrelation (Cleland and Sethupathy, 2006; Cleland et al., 2007) was omitted for simplicity, this intrinsic inhibition nevertheless generated a modest decorrelation (**Figure 2A**, MC/PNs). The matrix of projections from MC/PNs to PCs was sparse (5% of possible connections, randomly determined) and initially comprised only weak synaptic interactions; consequently, PCs initially responded weakly, and relatively broadly, to odorant stimulation (**Figure 2A**, PC, *naive*). Specifically, whereas OSNs responded with varying degrees of activation to an average of 69 ± 2% of randomly chosen complex odorants, MC/PNs responded to 24 ± 2% and PCs initially responded to 30 ± 5% of these odorants.

CONDITIONED ODOR RESPONSES IN MODEL PC ARE SPARSE AND SELECTIVE

Olfactory conditioning was simulated by presenting an odorant to the model for an epoch of 20–30 cycles of the underlying gamma oscillation, corresponding to a stimulus presentation of 500–750 ms in rodents or 1000–1500 ms in locusts or bees (due

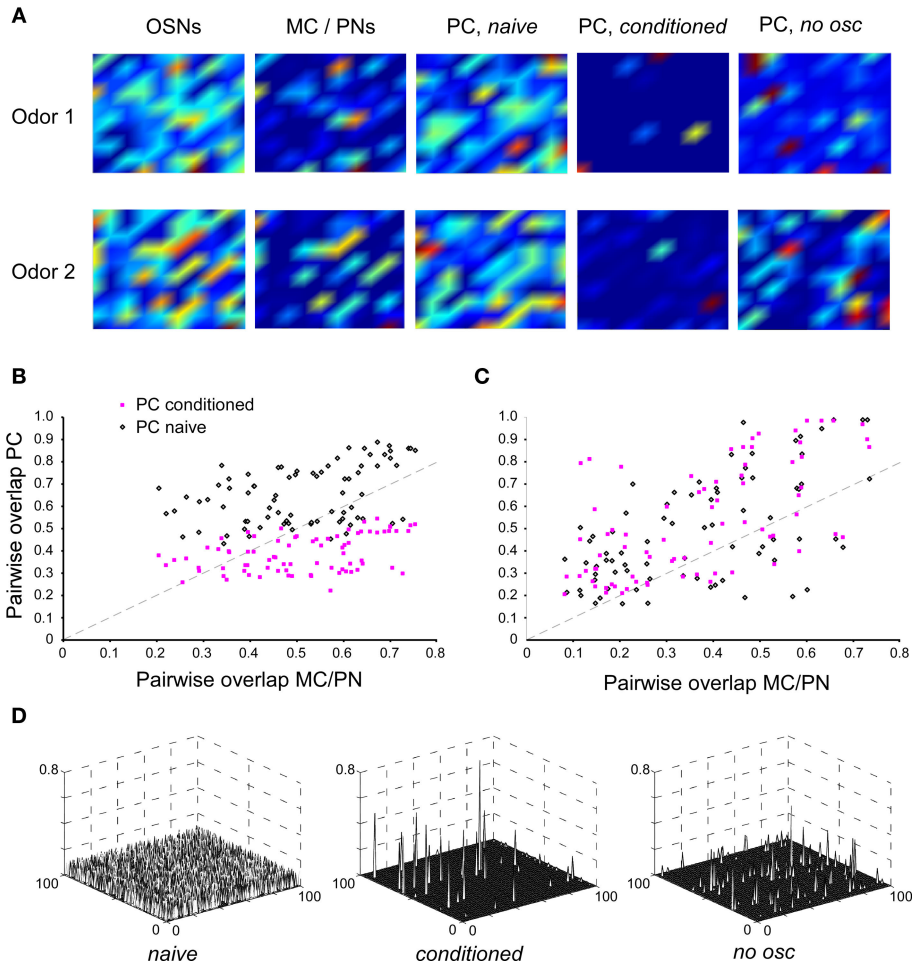

FIGURE 2 | Effects of single odor learning in PC and its dependence on MC/PN precedence coding. (A) Color–contour plots of odor-evoked activity patterns in each layer of the model. The neurons in each layer are displayed in a 10×10 matrix, with warmer colors indicating higher activation levels. Plots were smoothed using Matlab's built-in interpolation function. Two random odors, Odor 1 and Odor 2, were chosen for this example. First, each odor was presented for 20 gamma cycle periods (with the STDP learning rule disabled) and the resulting activity levels (total number of spikes in each neuron during the stimulus application) were measured and averaged. In the OSN layer, both odorants evoked relatively diffuse, overlapping patterns of activity; a slightly less diffuse pattern was observed in the MC/PN layer. In the naïve PC layer, odor activity was again highly broad and diffuse. The network was then conditioned by presenting Odor 1 for 20 gamma cycle periods with the STDP rule turned on. Subsequently, both odorants were presented again for 20 cycles with the learning rule disabled and the evoked activity measured. After conditioning, the PC network responded sparsely to the two odorants with highly decorrelated, non-overlapping patterns (PC, *conditioned*). The same procedure was then followed using a network in which oscillations were reduced substantially by interrupting the inhibitory feedback loop, thus disrupting the spike precedence code. Post-conditioning activation patterns in the PC in the absence of MC/PN oscillations were substantially more diffuse and overlapping (PC, *no osc*). **(B)** Effect of conditioning on pairwise overlap between odorants in the PC with MC/PN oscillations intact. Eighty random pairs of odorants were chosen; in each case the network was conditioned using one odorant of the pair. The graph depicts the degree of overlap between PC response patterns as a function of the overlap in MC/PN response patterns before (black open diamonds) and after (pink solid squares) conditioning. The dotted line indicates the diagonal. **(C)** Effect of conditioning on pairwise overlap between odorants in the PC with reduced oscillations in the MC/PN layer. Eighty random pairs of odorants were chosen; in each case the network was conditioned using one odorant of the pair. The graph depicts the degree of overlap between PC response patterns as a function of the overlap in MC/PN response patterns before (black open diamonds) and after (pink solid squares) conditioning. The dotted line indicates the diagonal. In the absence of MC/PN oscillations, the PC representation is not systematically decorrelated with respect to the MC/PN representation, either before or after conditioning. **(D)** Synaptic weight matrices from all MC/PN neurons to all PC neurons (100x100) in the naïve state, after normal conditioning (*conditioned*), and after conditioning in the absence of MC/PN oscillations (*no osc*).

to the slower oscillations exhibited by these insects). Comparable levels of learning also could be obtained using fewer cycles with a greater learning rate, or vice versa; the important criterion is that conditioning must persist for enough gamma cycles to enable extraction of the precedence code by the STDP learning rule. Importantly, after conditioning, the average number of complex odorants to which individual PC cells responded decreased ~3-fold, to $11 \pm 3\%$, rendering cortical odor representations significantly sparser than those mediated by earlier layers. To measure the effect of this conditioning on the degree of overlap between odor representations, the following procedure was followed. First, a "naive" network was constructed with parameters chosen around the values

Table 1| Mean parameters for network simulations.

NEURONS				
Olfactory sensory neurons (OSN)	$\tau = 5.0$ ms	$\theta_{min} = 0.0$	$\theta_{max} = 1.0$	
Local interneuron (HomoLN)	$\tau = 5.0$ ms	$\theta_{min} = 0.0$	$\theta_{max} = 4.0$	
Mitral cells/projection neurons (MC/PN)	$\tau = 2.0$ ms	$\theta_{min} = -1.0$	$\theta_{max} = 20.0$	
Cortical/MB neurons (PC)	$\tau = 5.0$ ms	$\theta_{min} = 0.0$	$\theta_{max} = 10.0$	
SYNAPSES				
Afferent, OSN to MC/PN	$g_{max} = 1.0$; $w_{MC,OSN} = 0.14$	$E_N = 70$	$\tau_1 = 1.0$	$\tau_2 = 2.0$
Afferent, OSN to HomoLN	$g_{max} = 1.0$; $w_{hLN,OSN} = 0.015$	$E_N = 70$	$\tau_1 = 1.0$	$\tau_2 = 2.0$
HomoLN inhibitory feedback	$g_{max} = 1.0$; $w_{hLN-hLN} = 0.5$ (*normal*) or 0.1 (*reduced oscillations*)	$E_N = -10$	$\tau_1 = 4.0$	$\tau_2 = 8.0$
HomoLN to MC/PN	$g_{max} = 1.0$; $w_{MC,hLN} = 0.2$ (*normal*) or 0.05 (*reduced oscillations*)	$E_N = -10$	$\tau_1 = 4.0$	$\tau_2 = 8.0$
MC/PN to PC (*initial value*)	$g_{max} = 1.0$; $w_{PC,MC} = 0.003$	$E_N = 70$	$\tau_1 = 1.0$	$\tau_2 = 2.0$
STDP LEARNING RULE				
MC/PN to PC synapse	$\tau+ = 5$ ms	$\tau- = 5$ ms	$A+ = 0.6$	$A- = -0.4$

A new network was created for each simulation; for each such network, all parameter values were determined randomly from a uniform distribution (±10%) around these mean values. The instantaneous spiking probability for each cell type is a continuous, bounded function of the membrane potential with a threshold θ_{min} and a saturation value θ_{max}. Omega values (w_{ij}) designate synaptic weights, and values of E_N designate synaptic reversal potentials. τ designates the membrane time constant, τ_1 and τ_2 the synaptic time constants, and $\tau+$ and $\tau-$ the time constants of the STDP associative learning rule. A+ and A– determine the STDP learning rates.

detailed in **Table 1** (see Materials and Methods), and randomized pairs of complex odor presentations were simulated. The overlap between the representations of these odorant pairs at the OSN level ranged from 40 to 93% with a mean overlap of 74 ± 0.8%, replicating typical experimental data for pairs of structurally related odorants (Meister and Bonhoeffer, 2001; Stettler and Axel, 2009). This overlap was reduced at the level of MC/PN spiking outputs, ranging from 20 to 82% with an average overlap of 50 ± 1.8%. In the naïve PC network, the overlap between pairs of odor representations *increased*, ranging from 43 to 88% with an average overlap of 65 ± 1.5% owing to the weak and randomly distributed initial connections between MC/PNs and PCs.

Next, one of the odorants in the pair was presented for a conditioning epoch, after which both odorants were again presented to the newly conditioned network and overlaps between the two representations in the PC layer were recalculated (**Figure 2A**, PC, *conditioned*). After conditioning, overlaps between pairs of representations ranged from 22 to 55% with an average of 39 ± 1.0%, reasonably replicating the overlap between the representations of structurally similar odorant pairs observed in piriform cortex (Stettler and Axel, 2009). The difference between the overlaps in naïve and post-conditioning odorant representations was highly significant (paired samples *t*-test; $p < 0.01$; **Figure 2B**).

PRECEDENCE CODE IS REQUIRED FOR DECORRELATION VIA STDP

As illustrated in **Figure 1D**, the STDP synaptic learning rule requires both sufficiently dense presynaptic spiking input to evoke postsynaptic action potentials and a common singular or periodic time reference that can disambiguate leading from lagging spikes, e.g., by binning them into a phase-constrained window with respect to the underlying gamma oscillation. Hence, in the present model, if the presynaptic neurons were not phase-constrained by gamma oscillations then they would not generate a coherent, readable precedence code; consequently, the STDP rule then should be unable to extract the information necessary to decorrelate odor representations in the PC layer. We tested this hypothesis by reducing the oscillatory drive onto the MC/PN neurons to a tonic inhibition, while ensuring that the overall firing rate of these neurons was not dramatically changed, thereby replicating the experimental protocol of Stopfer et al. (1997). This was achieved by reducing GABAergic inhibition in the model to 25% of its original value, reducing the feedback autoinhibition of the inhibitory interneuron and decreasing its oscillatory power while simultaneously weakening its inhibition of MC/PN neurons to maintain their average firing rates. While the average firing rates of MC/PN neurons did not change (*t*-test; $p > 0.05$; **Figure 1E**, left), the pairwise synchronization between MC/PN neurons was significantly reduced (*t*-test; $p < 0.01$; **Figure 1E**, right). Whereas postsynaptic spikes were still evoked in PC neurons, and the STDP learning rule still modified synaptic strengths and cortical representations accordingly, learning in this layer was weak and highly disorganized as a result of the loss of spike precedence information (**Figure 2A**, PC, *no osc*). Specifically, in the absence of the oscillation-driven phasing of MC/PN action potentials, measured overlaps between pairs of representations in the MC/PN layer ranged from 8 to 59% with an average overlap of 33 ± 1.9% (a somewhat lower value than in the oscillatory condition owing to the adjustments needed to maintain common MC/PN spike rates). Measured overlaps in the naïve PC layer (before conditioning) under these conditions ranged from 16 to 98% with an average overlap of 46 ± 2.6%, an increase in overlap comparable to that occurring under oscillatory conditions. However, after conditioning, in the absence of the oscillation-driven phasing of action potentials, measured overlaps increased still further, ranging from 21 to 94% with an average overlap of 53 ± 2.6% (**Figure 2C**). Pairwise synaptic weight matrices after conditioning reveal STDP-dependent plasticity in both the *conditioned* and *no osc* cases, compared to the naïve state (**Figure 2D**); however, in the absence of a coherent precedence code, STDP-dependent learning in the PC layer was disorganized, and consequently increased, rather than reduced, the similarities among different odor representations (**Figure 2C**). The decorrelation of odor representations by

post-bulbar STDP-based learning consequently depends on, and is selective for, spike precedence coding based on the metric proposed to exist in MC/PNs.

DECORRELATION OF HONEYBEE ANTENNAL LOBE ODOR REPRESENTATIONS

To further test the olfactory decorrelation mechanism described above, we adjusted the model to incorporate natural odor-evoked glomerular input patterns obtained from calcium imaging of the honeybee AL (Sachse and Galizia, 2003; Linster et al., 2005). The number of glomeruli in the model was reduced to 30, corresponding to the number for which calcium imaging data in response to stimulation with a homologous odor series of straight-chain aliphatic alcohols could be obtained (Sachse and Galizia, 2003). To adjust for this smaller network size, the projection matrix density from MC/PN to PC neurons was increased so that each MC/PN targeted 10% of PC neurons. The local interneuron in the model directly corresponds in the honeybee AL to a morphologically distinct class of local interneurons termed homoLNs (Fonta et al., 1993), which receive excitatory input from all glomeruli and inhibit all PNs in a homogeneous manner. Consistent with the present model architecture, oscillatory dynamics and phase-locking in the AL are dependent on homoLN inhibitory feedback connections, and disappear when these connections are blocked, whereas other inhibitory circuits in the honeybee and locust AL are spared (MacLeod and Laurent, 1996; Stopfer et al., 1997).

The patterns of OSN sensitivity to different odorants were directly derived from published glomerular calcium-imaging data in honeybees (Sachse and Galizia, 2003; courtesy of G. Galizia). Specifically, the model was stimulated with inputs corresponding to the patterned glomerular responses evoked by 1-hexanol, 1-heptanol, 1-octanol, and 1-nonanol (**Figure 3A**), and generated MC/PN and naïve PC network representations as described above. To simulate the proboscis extension training used in honeybee conditioning studies (Bhagavan and Smith, 1997; Laska et al., 1999; Guerrieri et al., 2005), the model was then stimulated for 20 oscillatory cycles with the glomerular hexanol pattern while synaptic plasticity between MC/PNs and PC neurons was active (Linster and Cleland, 2001; Cleland and Linster, 2002). After conditioning, the network was again stimulated with patterned glomerular inputs corresponding to each of the four odorants and the pairwise overlaps between responses to hexanol and responses to the other three odorants in the cortical layer were calculated. This phase corresponded to extinction trials during which the behavioral responses to the conditioned odor (hexanol) and novel test odors (heptanol, octanol, nonanol) are tested (Bhagavan and Smith, 1997; Laska et al., 1999; Guerrieri et al., 2005). The relative response magnitude to conditioned and test odors is a measure of odor discrimination. We performed this conditioning study twice: first with fast oscillations intact and then again with reduced feedback inhibition to the homoLN such that oscillations were abolished and MC/PN spike times were desynchronized on this timescale.

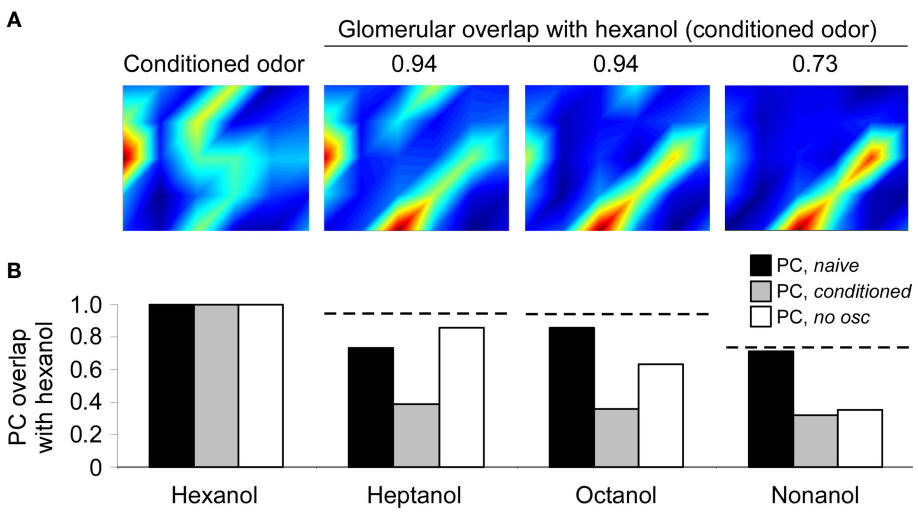

FIGURE 3 | Progressive decorrelation of odor representations via learning in the honeybee olfactory system. (A) Glomerular input patterns evoked by the odorants hexanol, heptanol, octanol, and nonanol as measured by calcium imaging of the honeybee antennal lobe (AL; Sachse and Galizia, 2003). The activation levels of the 30 glomeruli modeled are depicted in a 6×5 array that does not correspond to the anatomical arrangement of glomeruli on the AL. The degree of overlap (normalized dot product) between the glomerular-layer representations of hexanol and each of the other odors are indicated above the corresponding activation patterns. **(B)** Effects on odor representations by conditioning the network with hexanol. Overlaps between the representations of hexanol (the conditioned odor) and each of the other three test odors (heptanol, octanol, and nonanol) in PC neurons were calculated before (*PC, naive*) and after conditioning with hexanol (*PC, conditioned*). Overlaps were also calculated after conditioning using a network in which AL oscillations were substantially reduced as described above (*PC, no osc*). Because real odor input data were used to drive the model, each stimulus was presented only once (hence no error bars). Conditioning in the presence of oscillations sharply reduced the overlap between hexanol and each of the three test odorants. In the absence of oscillations, only the most dissimilar test odorant – nonanol – was decorrelated to the same extent. This indicates that spike timing-dependent decorrelation primarily affects highly similar odorants, as has been demonstrated behaviorally in honeybees (Stopfer et al., 1997). For purposes of comparison, dotted horizontal lines depict the degree of overlap with hexanol measured in the glomerular layer (as listed in **A**).

Odor-evoked representations in the naïve PC network were broad, and overlapped with the representations of similar odorants to roughly the same extent as in the glomerular layer (**Figure 3B**). After conditioning with hexanol, the pairwise overlaps between hexanol and each other test odor were strongly reduced (decorrelated) in the PC representation. This decorrelation replicates the pattern observed when honeybees' responses to structurally and perceptually similar odorants are measured after conditioning to sucrose rewards in the proboscis extension paradigm (Bhagavan and Smith, 1997; Laska et al., 1999; Guerrieri et al., 2005). In contrast, when oscillations and spike synchronization in the OB/AL were impaired, the overlaps between hexanol and highly similar odorants (heptanol, octanol) were substantially larger, exhibiting relatively little decorrelation with respect to the naïve representations. In contrast, the overlap between hexanol and the least-similar test odorant (nonanol) was reduced in the conditioned PC with or without the presence of oscillations, suggesting that the lower initial overlap between these odorants enabled sufficient decorrelation of these patterns even in the absence of oscillations. This similarity-dependent profile of responses is consistent with behavioral observations in honeybees demonstrating that abolishing oscillations in the AL during odor conditioning impairs bees' and moths' capacity to discriminate between highly similar, but not moderately similar or dissimilar, odorants (Stopfer et al., 1997; Mwilaria et al., 2008; see also Linster and Cleland, 2001; Cleland and Linster, 2002).

DISCUSSION

Second-order sensory neurons in the vertebrate and insect olfactory systems exhibit spiking activity that is phase-locked to underlying LFP oscillations, indicating a transformation in odor representations to a spike timing-based metric. Among candidate metrics for odor representation at this level, a simple spike precedence code, initiated by active sampling and maintained by intrinsic oscillations within the OB/AL network, is suggested. Whereas the first stage of post-sampling processing of odor representations appears to decorrelate odor representations with respect to their physical similarities via the selective silencing of moderately activated MC/PNs (reviewed in Cleland, 2010), the second stage model depicted herein further decorrelates odor representations not by silencing additional MC/PNs, but via the selective and progressive reduction of these neurons' capacity to influence the activity of specific post-synaptic PC neurons, resulting in a progressively sharper and more durable odor representation in this third-order neuronal population. This selectivity for correlated, precedent spikes also enables the PC to disregard the disorganized background spiking of MC/PNs that are neither substantially activated nor inhibited by odorants. Interestingly, it also could explain the observed psychophysical phenomenon in which increased odorant concentrations improve the rate and selectivity of odor learning (Yue et al., 2004; Wei et al., 2006; Cleland et al., 2009). Note that the proposed mechanism is not the only means by which representations could be decorrelated at this synapse: modulation of firing threshold or a sparsening of inputs by creating a sparser connectivity matrix would also achieve a basic decorrelation of all patterns. However, neither would exploit the spike dynamics observed in MC/PN neurons or decorrelate specific representations of interest from all others.

How well is this model of mitral cell precedence coding supported by electrophysiological and behavioral data? Mitral cells exhibit substantial background activity, particularly in awake animals (Rinberg et al., 2006); responses to odor stimulation evoke a range of qualitatively different initial responses from no effect, to inhibition (a common effect) to relatively fast excitation (Hamilton and Kauer, 1989; Wellis et al., 1989). A substantial fraction of odor-activated mitral cells exhibit phase-locked spiking (Kashiwadani et al., 1999; Buonviso et al., 2003; Lagier et al., 2004); in anesthetized, freely breathing (~2 Hz) rats, it has been estimated that 31% of mitral cells that are not silenced by a given odor presentation respond with gamma phase-locked spiking (David et al., 2009). Moreover, in studies mapping mitral cells' chemoreceptive fields, the "best" odorants that map to the central peak of a given cell's receptive field tend to evoke spikes at substantially shorter latencies than do odorants to which that cell is less well tuned (Wellis et al., 1989; Mori et al., 1999; Kaluza and Breer, 2000; Fletcher and Wilson, 2003; Stopfer et al., 2003; Friedrich et al., 2004), thereby creating the substrate for a precedence code based on odor quality tuning. While most of these studies measured spike latency on the respiratory (theta-band) timescale, there also is evidence for spike phasing with respect to fast oscillations (David et al., 2009). In the insect olfactory system, there is no direct evidence that PN spike phase is modulated by a cell's level of activation, although the transformation of temporal synchronization patterns into sparse spatial representations has been experimentally described (Perez-Orive et al., 2002).

Spike latency codes for odor quality representation have been proposed in a number of theoretical studies, though to different ends (Fort and Rospars, 1992; Hopfield, 1996; White et al., 1998; Schaefer et al., 2006). We here show how such a precedence code among second-order olfactory neurons could be read out and further processed using STDP to create sparse, plastic cortical representations comparable to those demonstrated experimentally (Roesch et al., 2007). The simulations presented here correspond to behavioral studies showing that, in a perceptual learning paradigm, repeated exposure to one or two odorants increases the perceptual contrast between these odorants and novel test odorants (Mandairon et al., 2006; **Figure 2** in the present manuscript). These effects of perceptual learning persist for less than 2 weeks; within this time window, repeated exposure to a new odorant can modify the perceptual changes due to a previous exposure. As we here make no provision for associating particular odors with reward or other contingencies, the simulations presented here do not address the larger question of long-term olfactory learning, by which a sparse functional projection matrix between bulb and cortex is formed and modified in response to a complex, slowly changing odor environment.

ACKNOWLEDGMENTS

We thank Giovanni Galizia for the use of calcium imaging data gathered in his laboratory. This work was supported by grants R03DC007725, R01DC009948, and R01DC008702 from the National Institute on Deafness and Communication Disorders (NIDCD).

REFERENCES

Abraham, N. M., Egger, V., Shimshek, D. R., Renden, R., Fukunaga, I., Sprengel, R., Seeburg, P. H., Klugmann, M., Margrie, T. W., Schaefer, A. T., and Kuner, T. (2010). Synaptic inhibition in the olfactory bulb accelerates odor discrimination in mice. *Neuron* 65, 399–411.

Ardid, S., Wang, X. J., Gomez-Cabrero, D., and Compte, A. (2010). Reconciling coherent oscillation with modulation of irregular spiking activity in selective attention: gamma-range synchronization between sensory and executive cortical areas. *J. Neurosci.* 30, 2856–2870.

Beshel, J., Kopell, N., and Kay, L. M. (2007). Olfactory bulb gamma oscillations are enhanced with task demands. *J. Neurosci.* 27, 8358–8365.

Bhagavan, S., and Smith, B. H. (1997). Olfactory conditioning in the honey bee, *Apis mellifera*: effects of odor intensity. *Physiol. Behav.* 61, 107–117.

Buonviso, N., Amat, C., Litaudon, P., Roux, S., Royet, J. P., Farget, V., and Sicard, G. (2003). Rhythm sequence through the olfactory bulb layers during the time window of a respiratory cycle. *Eur. J. Neurosci.* 17, 1811–1819.

Cassenaer, S., and Laurent, G. (2007). Hebbian STDP in mushroom bodies facilitates the synchronous flow of olfactory information in locusts. *Nature* 448, 709–713.

Cleland, T. A. (2010). Early transformations in odor representation. *Trends Neurosci.* 33, 130–139.

Cleland, T. A., Johnson, B. A., Leon, M., and Linster, C. (2007). Relational representation in the olfactory system. *Proc. Natl. Acad. Sci. U.S.A.* 104, 1953–1958.

Cleland, T. A., and Linster, C. (2002). How synchronization properties among second-order sensory neurons can mediate stimulus salience. *Behav. Neurosci.* 116, 212–221.

Cleland, T. A., Narla, V. A., and Boudadi, K. (2009). Multiple learning parameters differentially regulate olfactory generalization. *Behav. Neurosci.* 123, 26–35.

Cleland, T. A., and Sethupathy, P. (2006). Non-topographical contrast enhancement in the olfactory bulb. *BMC Neurosci.* 7, 7. doi: 10.1186/1471-2202-7-7.

David, F. O., Hugues, E., Cenier, T., Fourcaud-Trocme, N., and Buonviso, N. (2009). Specific entrainment of mitral cells during gamma oscillation in the rat olfactory bulb. *PLoS Comput. Biol.* 5, e1000551. doi: 10.1371/journal.pcbi.1000551.

Desmaisons, D., Vincent, J. D., and Lledo, P. M. (1999). Control of action potential timing by intrinsic subthreshold oscillations in olfactory bulb output neurons. *J. Neurosci.* 19, 10727–10737.

Fletcher, M. L., and Wilson, D. A. (2003). Olfactory bulb mitral-tufted cell plasticity: odorant-specific tuning reflects previous odorant exposure. *J. Neurosci.* 23, 6946–6955.

Fonta, C., Sun, X., and Masson, C. (1993). Morphology and spatial distribution of bee antennal lobe interneurons responsive to odours. *Chem. Senses* 18, 101–119.

Fort, J. C., and Rospars, J. P. (1992). Modelling of the qualitative discrimination of odours in the first two layers of olfactory system by Jutten and Herault algorithm. *CR Acad. Sci. III* 315, 331–336.

Friedrich, R. W., Habermann, C. J., and Laurent, G. (2004). Multiplexing using synchrony in the zebrafish olfactory bulb. *Nat. Neurosci.* 7, 862–871.

Fries, P., Nikolic, D., and Singer, W. (2007). The gamma cycle. *Trends Neurosci.* 30, 309–316.

Gray, C. M., and Singer, W. (1989). Stimulus-specific neuronal oscillations in orientation columns of cat visual cortex. *Proc. Natl. Acad. Sci. U.S.A.* 86, 1698–1702.

Guerrieri, F., Schubert, M., Sandoz, J. C., and Giurfa, M. (2005). Perceptual and neural olfactory similarity in honeybees. *PLoS Biol.* 3, e60. doi: 10.1371/journal.pbio.0030060.

Guyonneau, R., VanRullen, R., and Thorpe, S. J. (2005). Neurons tune to the earliest spikes through STDP. *Neural Comput.* 17, 859–879.

Hajos, N., and Paulsen, O. (2009). Network mechanisms of gamma oscillations in the CA3 region of the hippocampus. *Neural Netw.* 22, 1113–1119.

Hamilton, K. A., and Kauer, J. S. (1989). Patterns of intracellular potentials in salamander mitral/tufted cells in response to odor stimulation. *J. Neurophysiol.* 62, 609–625.

Hopfield, J. J. (1995). Pattern recognition computation using action potential timing for stimulus representation. *Nature* 376, 33–36.

Hopfield, J. J. (1996). Transforming neural computations and representing time. *Proc. Natl. Acad. Sci U.S.A.* 93, 15440–15444.

Illig, K. R., and Haberly, L. B. (2003). Odor-evoked activity is spatially distributed in piriform cortex. *J. Comp. Neurol.* 457, 361–373.

Johnson, D. M., Illig, K. R., Behan, M., and Haberly, L. B. (2000). New features of connectivity in piriform cortex visualized by intracellular injection of pyramidal cells suggest that "primary" olfactory cortex functions like "association" cortex in other sensory systems. *J. Neurosci.* 20, 6974–6982.

Kaluza, J. F., and Breer, H. (2000). Responsiveness of olfactory neurons to distinct aliphatic aldehydes. *J. Exp. Biol.* 203, 927–933.

Kashiwadani, H., Sasaki, Y. F., Uchida, N., and Mori, K. (1999). Synchronized oscillatory discharges of mitral/tufted cells with different molecular receptive ranges in the rabbit olfactory bulb. *J. Neurophysiol.* 82, 1786–1792.

Kay, L. M., Beshel, J., Brea, J., Martin, C., Rojas-Libano, D., and Kopell, N. (2009). Olfactory oscillations: the what, how and what for. *Trends Neurosci.* 32, 207–214.

Kay, L. M., and Freeman, W. J. (1998). Bidirectional processing in the olfactory-limbic axis during olfactory behavior. *Behav. Neurosci.* 112, 541–553.

Koehl, M. A., Koseff, J. R., Crimaldi, J. P., McCay, M. G., Cooper, T., Wiley, M. B., and Moore, P. A. (2001). Lobster sniffing: antennule design and hydrodynamic filtering of information in an odor plume. *Science* 294, 1948–1951.

Lagier, S., Carleton, A., and Lledo, P. M. (2004). Interplay between local GABAergic interneurons and relay neurons generates gamma oscillations in the rat olfactory bulb. *J. Neurosci.* 24, 4382–4392.

Laska, M., Galizia, C. G., Giurfa, M., and Menzel, R. (1999). Olfactory discrimination ability and odor structure-activity relationships in honeybees. *Chem. Senses* 24, 429–438.

Laurent, G. (1999). A systems perspective on early olfactory coding. *Science* 286, 723–728.

Laurent, G., and Davidowitz, H. (1994). Encoding of olfactory information with oscillating neural assemblies. *Science* 265, 1872–1875.

Linster, C., and Cleland, T. A. (2001). How spike synchronization among olfactory neurons can contribute to sensory discrimination. *J. Comput. Neurosci.* 10, 187–193.

Linster, C., Henry, L., Kadohisa, M., and Wilson, D. A. (2007). Synaptic adaptation and odor-background segmentation. *Neurobiol. Learn Mem.* 87, 352–360.

Linster, C., Menon, A. V., Singh, C. Y., and Wilson, D. A. (2009). Odor-specific habituation arises from interaction of afferent synaptic adaptation and intrinsic synaptic potentiation in olfactory cortex. *Learn Mem.* 16, 452–459.

Linster, C., Sachse, S., and Galizia, C. G. (2005). Computational modeling suggests that response properties rather than spatial position determine connectivity between olfactory glomeruli. *J. Neurophysiol.* 93, 3410–3417.

MacLeod, K., and Laurent, G. (1996). Distinct mechanisms for synchronization and temporal patterning of odor-encoding neural assemblies. *Science* 274, 976–979.

Mandairon, N., and Linster, C. (2009). Odor perception and olfactory bulb plasticity in adult mammals. *J. Neurophysiol.* 101, 2204–2209.

Mandairon, N., Stack, C., Kiselycznyk, C., and Linster, C. (2006). Enrichment to odors improves olfactory discrimination in adult rats. *Behav. Neurosci.* 120, 173–179.

Martin, C., Beshel, J., and Kay, L. M. (2007). An olfacto-hippocampal network is dynamically involved in odor-discrimination learning. *J. Neurophysiol.* 98, 2196–2205.

Masquelier, T., Hugues, E., Deco, G., and Thorpe, S. J. (2009). Oscillations, phase-of-firing coding, and spike timing-dependent plasticity: an efficient learning scheme. *J. Neurosci.* 29, 13484–13493.

Meister, M., and Bonhoeffer, T. (2001). Tuning and topography in an odor map on the rat olfactory bulb. *J. Neurosci.* 21, 1351–1360.

Mori, K., Nagao, H., and Yoshihara, Y. (1999). The olfactory bulb: coding and processing of odor molecule information. *Science* 286, 711–715.

Mwilaria, E. K., Ghatak, C., and Daly, K. C. (2008). Disruption of GABAA in the insect antennal lobe generally increases odor detection and discrimination thresholds. *Chem. Senses* 33, 267–281.

Nase, G., Singer, W., Monyer, H., and Engel, A. K. (2003). Features of neuronal synchrony in mouse visual cortex. *J. Neurophysiol.* 90, 1115–1123.

Neville, K. R., and Haberly, L. B. (2003). Beta and gamma oscillations in the olfactory system of the urethane-anesthetized rat. *J. Neurophysiol.* 90, 3921–3930.

Nusser, Z., Kay, L. M., Laurent, G., Homanics, G. E., and Mody, I. (2001). Disruption of GABA(A) receptors on GABAergic interneurons leads to increased oscillatory power in the olfactory bulb network. *J. Neurophysiol.* 86, 2823–2833.

Panzeri, S., Brunel, N., Logothetis, N. K., and Kayser, C. (2009). Sensory neural codes using multiplexed temporal scales. *Trends Neurosci.* 33, 111–120.

Perez-Orive, J., Mazor, O., Turner, G. C., Cassenaer, S., Wilson, R. I., and Laurent, G. (2002). Oscillations and sparsening of odor representations in the mushroom body. *Science* 297, 359–365.

Poo, C., and Isaacson, J. S. (2009). Odor representations in olfactory cortex: "sparse" coding, global inhibition, and oscillations. *Neuron* 62, 850–861.

Rinberg, D., Koulakov, A., and Gelperin, A. (2006). Sparse odor coding in awake behaving mice. *J. Neurosci.* 26, 8857–8865.

Roesch, M. R., Stalnaker, T. A., and Schoenbaum, G. (2007). Associative encoding in anterior piriform cortex versus orbitofrontal cortex during odor discrimination and reversal learning. *Cereb. Cortex* 17, 643–652.

Rubin, D. B., and Cleland, T. A. (2006). Dynamical mechanisms of odor processing in olfactory bulb mitral cells. *J. Neurophysiol.* 96, 555–568.

Sachse, S., and Galizia, C. G. (2003). The coding of odour-intensity in the honeybee antennal lobe: local computation optimizes odour representation. *Eur. J. Neurosci.* 18, 2119–2132.

Schaefer, A. T., Angelo, K., Spors, H., and Margrie, T. W. (2006). Neuronal oscillations enhance stimulus discrimination by ensuring action potential precision. *PLoS Biol.* 4, e163. doi: 10.1371/journal.pbio.0040163.

Schaefer, A. T., and Margrie, T. W. (2007). Spatiotemporal representations in the olfactory system. *Trends Neurosci.* 30, 92–100.

Sirota, A., Montgomery, S., Fujisawa, S., Isomura, Y., Zugaro, M., and Buzsaki, G. (2008). Entrainment of neocortical neurons and gamma oscillations by the hippocampal theta rhythm. *Neuron* 60, 683–697.

Song, S., Miller, K. D., and Abbott, L. F. (2000). Competitive Hebbian learning through spike-timing-dependent synaptic plasticity. *Nat. Neurosci.* 3, 919–926.

Stettler, D. D., and Axel, R. (2009). Representations of odor in the piriform cortex. *Neuron* 63, 854–864.

Stopfer, M., Bhagavan, S., Smith, B. H., and Laurent, G. (1997). Impaired odour discrimination on desynchronization of odour-encoding neural assemblies. *Nature* 390, 70–74.

Stopfer, M., Jayaraman, V., and Laurent, G. (2003). Intensity versus identity coding in an olfactory system. *Neuron* 39, 991–1004.

Uhlhaas, P. J., Pipa, G., Lima, B., Melloni, L., Neuenschwander, S., Nikolic, D., and Singer, W. (2009). Neural synchrony in cortical networks: history, concept and current status. *Front Integr. Neurosci.* 3: 17. doi: 10.3389/neuro.07.017.2009.

Wachowiak, M., Wesson, D. W., Pirez, N., Verhagen, J. V., and Carey, R. M. (2009). Low-level mechanisms for processing odor information in the behaving animal. *Ann. N.Y. Acad. Sci.* 1170, 286–292.

Wei, C. J., Linster, C., and Cleland, T. A. (2006). Dopamine D(2) receptor activation modulates perceived odor intensity. *Behav. Neurosci.* 120, 393–400.

Wellis, D. P., Scott, J. W., and Harrison, T. A. (1989). Discrimination among odorants by single neurons of the rat olfactory bulb. *J. Neurophysiol.* 61, 1161–1177.

White, J., Dickinson, T. A., Walt, D. R., and Kauer, J. S. (1998). An olfactory neuronal network for vapor recognition in an artificial nose. *Biol. Cybern.* 78, 245–251.

Yue, E. L., Cleland, T. A., Pavlis, M., and Linster, C. (2004). Opposing effects of D1 and D2 receptor activation on odor discrimination learning. *Behav. Neurosci.* 118, 184–190.

Conflict of Interest Statement: The authors declare that the research was conducted in the absence of any commercial or financial relationships that could be construed as a potential conflict of interest.

Received: 03 March 2010; accepted: 15 December 2010; published online: 28 December 2010.

*Citation: Linster C and Cleland TA (2010) Decorrelation of odor representations via spike timing-dependent plasticity. Front. Comput. Neurosci. **4**:157. doi: 10.3389/fncom.2010.00157*